

Fabrication technology for high light-extraction ultraviolet thin-film flip-chip (UV TFFC) LEDs grown on SiC

Burhan K. SaifAddin^{1*}, Abdullah Almogbel^{1,3}, Christian J. Zollner¹, Humberto Foronda¹, Ahmed Alyamani³, Abdulrahman Albadri³, Michael Iza¹, Shuji Nakamura^{1,2}, Steven P. DenBaars^{1,2}, and James S. Speck¹

¹Materials Department, UCSB, CA 93106, USA

²Department of Electrical and Computer Engineering, UCSB, CA 93106, USA

³King Abdulaziz City of Science and Technology (KACST), Saudi Arabia

*bks@ucsb.edu

Abstract

The light output of deep ultraviolet (UV-C) AlGaIn light-emitting diodes (LEDs) is limited due to their poor light extraction efficiency (LEE). To improve the LEE of AlGaIn LEDs, we developed a fabrication technology to process AlGaIn LEDs grown on SiC into thin-film flip-chip LEDs (TFFC LEDs) with high LEE. This process transfers the AlGaIn LED epi onto a new substrate by wafer-to-wafer bonding, and by removing the absorbing SiC substrate with a highly selective SF₆ plasma etch that stops at the AlN buffer layer. We optimized the inductively coupled plasma (ICP) SF₆ etch parameters to develop a substrate-removal process with high reliability and precise epitaxial control, without creating micromasking defects or degrading the health of the plasma etching system. The SiC etch rate by SF₆ plasma was ~46 μm/hr at a high RF bias (400 W), and ~7 μm/hr at a low RF bias (49 W) with very high etch selectivity between SiC and AlN. The high SF₆ etch selectivity between SiC and AlN was essential for removing the SiC substrate and exposing a pristine, smooth AlN surface. We demonstrated the epi-transfer process by fabricating high light extraction TFFC LEDs from AlGaIn LEDs grown on SiC. To further enhance the light extraction, the exposed N-face AlN was anisotropically etched in dilute KOH. The LEE of the AlGaIn LED improved by ~3X after KOH roughening at room temperature. This AlGaIn TFFC LED process establishes a viable path to high external quantum efficiency (EQE) and power conversion efficiency (PCE) UV-C LEDs.

Keywords: epi-transfer and heterogeneous integration technology, deep ultraviolet light-emitting diodes (UV-C LEDs), UV TFFC LEDs, light sources, light extraction efficiency, AlGaIn, AlN, semiconductor devices.

1. Introduction

AlGaIn ultraviolet light-emitting diodes (UV LEDs) and ultraviolet laser diodes (UV LDs) in the range of 265–280 nm are needed to develop novel disinfection and sterilizing technologies (water, air, and surfaces) to improve access to clean water [1–4], improve public health [5,6], and enable other biotech applications [7–10]. UV LEDs are a viable technology for replacing mercury gas discharge lamps in disinfection and biotechnology applications [11–18]. Hospitals, for example, reduced the rates of hospital-acquired drug-resistant infections by 25% using ultraviolet disinfection (via mercury lamps (254 nm)), as reported by various clinical trials [19,20]. Furthermore, the AlN or AlGaIn epi-transfer

and heterogeneous integration technology can be employed to enhance the performance of photodiodes (PDs) [21], high electron mobility transistors (HEMTs) [22,23], bulk acoustic resonators (BARs) [24–26], and high-aspect-ratio SiC microstructures and devices [27–30].

Researchers developing AlGaN LEDs have made significant progress in the last 30 years [11,18,31–44]; however, the technology is limited by light extraction efficiency (LEE) [45–54]. The LEE of AlGaN LEDs is less than that of InGaN blue LEDs for five main reasons. First, the absence of a transparent current spreading layer over p-GaN, such as indium tin oxide (ITO) for blue LEDs, requires the use of flip-chip (FC) LEDs architecture with a highly-reflective p-side down. Second, the poor conductivity of Mg-doped AlGaN necessitates the use of an optically absorbing p⁺-GaN layer for hole injection into the Mg-doped AlGaN and the formation of an ohmic p-contact; GaN has an absorption coefficient of $1.5 \times 10^5 \text{ cm}^{-1}$ at 275 nm [55]. Third, the reflectivity of ohmic p-contacts, is limited to ~70-80% , in the 265-280 nm range. Fourth, the light from the AlGaN MQW emitters at these wavelengths is ~40% transverse magnetic (TM) polarized [47,48,56–58], which propagates laterally; finite-difference time-domain (FDTD) calculations estimate that the extraction of TM emission is >10X less efficient than transverse electric (TE) polarization in typical volumetric FC LEDs [48] (in volumetric FC LEDs light has to travel through the transparent growth substrate) [48]. Lastly, the encapsulants used to enhance LEE in blue LEDs suffer low transparency, poor stability, and a low refractive index in deep ultraviolet LEDs [59–63].

The most commonly employed substrates for AlGaN UV-C LEDs are sapphire and AlN but they yield LEDs with low LEE. Although sapphire substrates are transparent, their thermal conductivity is limited, and they lack efficient ways to extract TM polarization because roughening the sidewalls of sapphire LEDs dies is challenging [46]. AlN substrates grown by physical vapor transport (PVT) are limited by an absorption around 264 nm (4.7 eV) with an absorption coefficient of about $\sim 35 \text{ cm}^{-1}$ [64] whereas hydride vapor phase epitaxy (HVPE) grown AlN substrates have less absorption ($\sim 10 \text{ cm}^{-1}$) [65]. Researchers have largely overlooked AlGaN LEDs grown on SiC substrates [66–74] because SiC absorbs strongly below its optical bandgap (3.2 eV and 3.0 eV for 4H-SiC and 6H-SiC, respectively), but this disadvantage can be overcome with a novel thin-film flip-chip (TFFC) LED architecture in which the SiC is removed with a highly selective SF₆ chemical plasma etch between SiC and AlN.

Growing AlN on SiC substrates is promising due to their similar crystallographic structure, polarity, chemical stability, and low lattice mismatch (0.8%) [75–80]. AlN grown on SiC with low threading dislocations has been demonstrated with MOCVD [78,81] and plasma-assisted MBE [71,76]. Furthermore, we demonstrate in this paper that AlGaN LEDs grown on SiC can be processed into thin-film LEDs with high LEE [82–85]; for example, FDTD simulations by Ryu et al. show that TM emission's LEE in textured thin-film LEDs is significantly higher (>6X) than in volumetric AlGaN FC-LEDs [48]. InGaN thin-film blue LEDs were developed with very high LEE using laser lift-off for substrate removal, N-face GaN KOH photoelectrochemical (PEC) roughening, and a p-side reflective mirror [86–88]. Several methods for laser lift-off of AlGaN UV-C LEDs

have been developed [89–94]; however, laser-induced melting of the Al in the dislocated interface of the AlN buffer layer in AlGaN LEDs causes more cracks than laser lift-off of the GaN buffer layer in InGaN LEDs [95] because the Al melts at 660 °C, whereas Ga melts at 30 °C [91]. Employing PEC etching to lift-off thin-film LEDs from their growth substrates [70,71] is more difficult with AlN than with GaN because N-face AlN etches anisotropically in KOH (without above-bandgap light assistance) considerably faster (~20x) than N-face GaN does [98]. Thus, KOH roughening can damage the active region before the lateral lift-off etch is completed.

In this paper, we demonstrate a process to fabricate high extraction efficiency TFFC LEDs grown on SiC. We characterize SiC and AlN etching using inductively coupled plasma (ICP) SF₆ plasma. The SF₆ gas flow, process pressure, and sample RF bias power were investigated to determine first-order trends between the etch parameters and the etch rates of SiC and AlN. Next, the etch parameters were optimized to develop a highly reliable SiC substrate-removal process with no micromasking defects and precise epitaxial control, without degrading the plasma etching system health. A highly selective SF₆ etch between SiC and AlN (90:1) was achieved which was essential for removing the SiC substrate and exposing a smooth AlN surface (roughness ~0.6 nm). We demonstrate high LEE thin-film flip chip (TFFC) AlGaN LEDs grown on SiC. We compare the power output of TFFC AlGaN LEDs before and after KOH roughening of the exposed AlN surface. The AlGaN LED's LEE improved by ~3X after roughening in KOH [0.25 M] for 70 sec at room temperature.

2. SiC substrate thinning characteristics

AlN was grown on quartered 2-inch 6H-SiC substrates (SiCrystal AG) by MOCVD as described elsewhere [81]. A one-step lapping process was used to thin the SiC substrates after bonding them to a carrier with high thermal conductivity (4.9 W/cm a-plane, 3.9 W/cm c-plane) with n- and p- bonding pads using Au/Au thermocompression bonding [73,74]. The SiC based samples were mounted episeide-down on a 2-inch stainless-steel chuck using a wax (that melts at 120 °C), which provides mechanical adhesion during lapping. The lapping process was performed using South Bay Technologies multipurpose lapping system (Model 920). The SiC growth substrates were thinned from 250 μm to 75 μm by lapping with a 9 μm Dia-Grid Diamond Disc (Allied High Tech Products, Inc.). The water-cooled lapping tool had a lapping rate of 29 μm/hr using 9 μm grit diamond discs. A summary of the thinning parameters is shown in Table 1. The lapping damage generated by lapping with a 9 μm grit was approximately 3 x 9 μm = 27 μm, which avoids damage to the active region. The mechanical lapping yields a total thickness variation (TTV) of about 15–20 μm across a quartered 2-inch wafer.

3. SF₆ etch chemistry characteristics

The SiC substrates were plasma etched in a Panasonic ICP etching system (E6261) using SF₆ plasma [67,68,101–103]. ICP etching systems have independent ICP and RF bias sources. The ICP plasma (generated by a current flowing in a planner coil above the etch chamber) power controls the ions and radicals densities. The RF bias power controls

the ions bombardment energy and thus is proportional to sputter (physical) etching. The samples were mounted episcide-down on a 6-inch carrier wafer using a vacuum diffusion pump fluid, which provides thermal conduction between the sample and the carrier wafer. The sample surface temperature depends on the lower electrode temperature and on the plasma ions' energies and densities. The lower electrode of the ICP system was backside cooled by pressurized He, and the carrier wafer temperature was kept at 11 °C during all etches. The 6-inch carrier wafer was a 1.5 mm thick fused silica wafer with a 100 nm Al backside coating to hold the fused silica carrier wafer to the electrostatic chuck. The chamber and carrier wafer were cleaned in O₂ plasma and then seasoned with a 2 min SF₆ etch at 1000 W ICP power and low RF bias (49 W). We found that chamber and carrier wafer seasoning suppressed the formation of SiC pillars. The SiC etch rates were determined by profilometry (Dektak) and scanning electron microscopy (SEM).

Etching SiC with SF₆ plasma produces the volatile products SiF₄, SiF₂, CF₂ and CF₄ [104]; the absence of etch-induced polymer generation renders the long etching (for several hours, if needed) consistent and reliable. Thus, long SF₆ etching does not need to be interrupted to clean the etch chamber because the etch chemistry does not cause polymer accumulation. However, the carrier wafer's temperature in the ICP etch chamber should be controlled during long etches because elevated temperatures can increase the SiC etch rate.

We developed a two step SF₆ ICP etch process to remove SiC: (1) high SiC etch rate process; (2) high selectivity SiC:AlN etch process. The two-step etch parameters are summarized in Table 2.

To achieve the highest etch rates of bulk SiC, we observed SiC etch rate as a function of SF₆ flow and process pressure. Figure 1(a) shows that the SiC etch rate increased as SF₆ flow increased, with improved etch uniformity. Figure 1(b) shows that the etch rate was sensitive to the process pressure. Increasing the process pressure, increases the ions' densities but decreases the ions' energies, by decreasing its mean free path. The SiC etch rate data in figure 2(b) shows that a chamber pressure of 1.33 Pa resulted in the highest SiC etch rate at the following process parameters: 1000 W ICP power, 400 W RF bias power, and 50 sccm SF₆ flow.

To achieve high etch selectivity, we utilized the fact that SiC etches chemically in SF₆, whereas AlN does not etch chemically in SF₆ and is only etched at a low rate by SF₆ sputter etching (at low RF bias). Figure 2(a) shows that the SiC etch rate increased as the RF bias power increased. At high RF bias power, SF₆ sputter etch dominates whereas at low RF bias (below 60 W), SF₆ chemical etch dominates and the sputter etch rate for SiC and AlN is very low. The etch rate at 400 W was about ~40 μm/hr when measured over 40 min and 46 μm/hr when measured over 2 hr. The SiC substrate was etched first at ~46 μm/hr over 1.2 hr to remove about 60 μm of SiC; the temperature of the He-cooled carrier wafer increased slightly from 11 °C to 15 °C. Achieving higher SiC etch rate is possible in plasma etch systems that have higher ICP power and RF bias power.

Figure 2(b) shows that the SiC:AlN etch selectivity was very sensitive to RF bias, especially below 60 W. . At high RF bias, the etch selectivity was low (10:1 at 400 W) because at this regime, sputter etching has low selectivity between SiC and AlN. On the other hand, the SiC:AlN etch selectivity increased significantly as the RF bias decreased below 60 W, where the SF₆ chemically etches SiC but does not etch AlN due to the formation of the low-volatility species AlF₃, which was demonstrated previously in studies of selective reactive ion etching of GaAs on AlGaAs and GaP on AlGaP in fluorine containing plasma [105–108]. However, the strong dependence of the SiC:AlN etch selectivity on the RF bias power decreased when the RF bias power was less than 47 W, as the SiC etch rate decreased more than the AlN etch rate did.

SiC:AlN etch selectivity is essential for removing the SiC substrate without damaging the active layer by stopping at the AlN buffer layer with precise epitaxial control. The etch selectivity was dependent on the substrate temperature (maintained at 11 °C), process pressure, and the RF bias power, especially in the 47–49 W region. For a thinned, quartered 2-inch SiC substrate with ~15–20 μm in TTV, a SiC:AlN etch selectivity of 90:1 at 49 W RF bias and 1.33 Pa was sufficient to reliably and selectively etch SiC and expose a pristine surface of N-face AlN. At a lower process pressure of 0.8 Pa, the SiC:AlN etch selectivity increased to 150:1. This indicates that the selectivity can be increased further by optimizing the process pressure. Senesky et al. [27] reported an SF₆ etch selectivity (at a low RF bias) of 16:1 (SiC:AlN) using AlN deposited with reactive sputtering; the higher bulk SiC etch selectivities obtained with MOCVD-grown AlN (at a low RF bias) indicate that AlN grown by MOCVD could replace Ni as a hard mask in fabricating high-aspect-ratio SiC microstructures and devices [28,29].

We optimized the SF₆ ICP etch to ensure that it removed the thick SiC substrate without producing micromasking defects on the thin-film LEDs surface and without degrading the plasma etching system health. First, we avoided the use of commonly used metal carriers inside the etch chamber (refer to Table 3). In ICP plasma etch systems, SF₆ etching is typically performed using a 6-inch Ni or Al carrier wafer because: both have low etch rates in SF₆ [101,109], as shown in Table 3. However, the use of metal carrier wafers increases micro-masking defects (which produces 40+ μm SiC pillars, as shown in figure 3(a)) that will not etch completely, even with the selective etch. Furthermore, sputtered metal from metal carriers can affect subsequent etches or cause electrical shorting [27], and require manual cleaning of the etch chamber after every etch. The use of fused silica (SiO₂) or sapphire carrier wafers minimized the micro-masking defects (SiC pillars) on the etched surface and did not affect the ICP etch chamber walls. The suppression of SiC pillars is shown in SEM images in figure 3(b). Selective etching of a SiC surface with suppressed micromasking defects exposed a smooth AlN surface (refer to figure 4(e) for an AFM scan of the exposed AlN surface with RMS roughness < 1 nm) that was free of SiC pillars, as shown in the optical and SEM micrographs of the TFFC LEDs in figure 5. Some literature indicates that the etch pressure requires optimization to remove SiC pillars; however, we found that pillar formation can be suppressed with appropriate selection of the carrier wafer, combined with the seasoning of both the carrier wafer and the etch chamber.

4. TFCC UV-C LED (278 nm) demonstration

The thin-film transfer technology was demonstrated on a high LEE TFCC UV-C LED, as shown in figures 4-6.

Figure 4 shows the process flow to fabricate TFCC LEDs from LED grown on SiC. The AlGa_N LED structure was first grown on a quartered 2-inch 6H-SiC substrate (SiCrystal AG) by MOCVD as reported elsewhere [85]. The LED structure is shown in figure 6(a) and consisted of AlN (3.2 μm), Al_{0.8}Ga_{0.2}N (180 nm), n-Al_{0.6}Ga_{0.4}N (1.1 μm), 278 nm MQWs 4x(Al_{0.39}Ga_{0.61}N/ Al_{0.6}Ga_{0.4}N), p-Al_{0.53}Ga_{0.47}N (50 nm), and p-GaN (5 nm). The samples were cleaved into 1.1 x 1.1 cm² samples and were processed into LEDs. The n-contact was V/Al/V/Au (20/80/20/200 nm); the p-contact was unannealed Ni/Al/Ni/Au (1/150/100/1000 nm) (refer to [85] for details). After a 3 min solvent clean and 30 sec O₂ plasma clean (100 W), the LEDs were bonded to a thermally conductive substrate (semi-insulating 4H-SiC, Cree, Inc.) with n- and p- bonding pads (20/1500 nm Ti/Au were deposited by e-beam). The samples were bonded using low-temperature Au/Au thermocompression bonding. A Finetech flip-chip bonder (FINEPLACER lambda) was employed for aligned wafer-to-wafer bonding. The bond was performed at 30 N/cm² for 5 min at 275 °C in air. Then, the samples were bonded further in custom-designed graphite fixtures that applied ~300 N/cm² pressure while the sample was annealed at 200 °C for 2 hr in air (the pressure was maintained during a 5 min cooldown); refer to Table 4 for a summary of the low-temperature Au/Au thermocompression bonding parameters. The 6H-SiC growth substrate was lapped mechanically to 75 μm and removed by a two-step SF₆ plasma etch, as previously described. Figure 5(a) shows plain-view optical micrograph images of processed UV LEDs with partially exposed AlN during an etch interrupt. The exposed TFCC LEDs had no visible cracks or chipping. The complete removal of SiC and exposure of pristine AlN surface was visible to the eye — a colorful interference pattern was observed as the light incident, and reflected from different surfaces in the TFCC LED interferes [110]. Also, the wettability of the surface changed as the N-face AlN was exposed. Namely, the surface of the etched carbon-face SiC was hydrophilic, and the surface of the exposed AlN was hydrophobic, as shown in figure 5(a). The TFCC LED contacts design is shown in figure 5(b) which shows a 5-finger topology for p-contact, surrounded by n-contact, with p-contact area of 0.093 mm². The 5-finger p-contact topology was adopted to avoid current crowding in the n-AlGa_N layer [111], which had a relatively high resistivity (~60 mΩ-cm²).

After complete removal of the SiC growth substrate, the suspended AlN/AlGa_N/n-AlGa_N thin-film in-between the TFCC LEDs, which is above the n- and p-pads (as shown in figure 5(b)), can be removed via a patterned hard mask (SiO₂) and KOH, or by etching a wider and deeper mesa around the LEDs mesa (into 80% of the AlN thickness) — before FC bonding. However, we relied on the residual tensile stress in the AlN/AlGa_N/n-AlGa_N film, which caused it to slightly concave upward [98]. Thus, after the TFCC LEDs were singulated, the n- and p- pads becomes accessible to wire bonding, as shown in figure 5(c). The TFCC LEDs were singulated by mechanical sawing using an ADT 7100 Dicing Saw. The TFCC LEDs were covered by photoresist for protection from the cooling/cleaning water jets that are needed during mechanical sawing. Subsequently, the TFCC LEDs were

mounted on TO headers using a Ni-Au epoxy from DEXTERIALS Corp., and the light output of the LEDs was measured in a 75 mm integrating sphere (Digital Instruments, Inc.).

Figure 6(b) compares the dependence of a TFFC LED's light output power (L) on the injected DC current (I) before and after optimized KOH roughening of the exposed AlN surface [85]. The slope of the power versus current increased by $\sim 3X$ after KOH roughening of the exposed AlN layer in dilute KOH (0.25 M) for 70 sec (refer to the bird's-eye-view SEM image of the resulting hexagonal pyramids in figure 6(c)). The LEE enhancement after KOH roughening was limited to $\sim 3X$ (as estimated from the enhancement in the L-I slope) due to the limited p-contact reflectivity and the use of a 5 nm p^+ -GaN layer (a strongly absorbing layer) to inject holes into the LED active region. Further LEE enhancement is possible without using p-GaN and by using a more reflective p-contacts. For example, the photoluminescence (PL) of MQW wells in an n-i-n structure (n-Al_{0.6}Ga_{0.4}N/286-nm-MQWs/n-Al_{0.6}Ga_{0.4}N/Al_{0.6}GaN/AlN) could be enhanced by $\sim 3.9X$ [112] after KOH roughening by using a highly reflective p-contact (a Pt/Al/Ni/Au p-contact with a Pt thickness of 0.26 nm and reflectivity of 90% at 286 nm was used to produce a $\sim 3.9X$ intensity enhancement in PL after KOH roughening).

The LEE of TM emissions in KOH-roughened TFFC LEDs are expected to be higher than in bulk FC LEDs. For example, Lee et al. studies on LEE in AlGaIn UV LEDs [113] showed that LEE from a PSS sapphire AlGaIn LED die was limited by sidewall roughness, more so than in InGaIn-based bulk FC LEDs, and that LEE from sidewalls is significant in thick (e.g., 300 μm thick sapphire) bulk FC AlGaIn LED but becomes negligible in relatively thin bulk FC AlGaIn LEDs (e.g., 90 μm thick sapphire). However, in TFFC LEDs, the contribution of sidewall emissions is negligible because the thin-film LED widths are much larger than its thickness, which is only 2–3 μm , and both TE and TM light emission couple into the roughened AlN surface; for example, FDTD simulations by Ryu et al. showed that the LEE of TM emission in roughened AlGaIn thin-film LEDs is significantly higher ($>6X$) than in bulk AlGaIn FC-LEDs [48]. The TE/TM emissions ratio depends on the MQWs strain and the Al composition in the wells and barriers [114–116]. We speculate that the strain state of the MQWs grown on SiC will be similar to MQWs grown on sapphire because (1) the AlN buffer layer is normally relaxed in both sapphire and SiC substrates, and therefore the AlGaIn MQWs are similarly compressively strained by the AlN lattice; and (2) the piezoelectric component due to thermal coefficient of expansion (TCE) mismatch (compressive in sapphire, and slightly tensile in SiC) between the AlN and AlGaIn layers is negated because it affects them similarly.

Estimating the LEE in unroughened thin-film LEDs could be challenging. For example, thin-film blue LEDs with KOH-roughened GaN buffer layers, ray tracing simulations estimate 13 % LEE for each single-pass extraction (6 bounces for full extraction) [117], whereas wave optics simulations estimate 31% LEE for each single-pass extraction (3 bounces for full extraction) [118]. We will discuss our estimates for the LEE of TFFC LEDs in a future publication.

After the optimized KOH roughening, the LED CW power was 7.8 mW at 95 mA, emitting at 278.5 nm, which yielded an EQE of 2%. Stable encapsulation [61] can further enhance

the LEE from TFFC LEDs; however, most resins absorb strongly below 330 nm and decompose over time, which renders them commercially unviable. A higher LEE for AlGaIn TFFC LEDs is also achievable if the p-GaN layer is replaced with a transparent hole injector [119–121] or if the reflectivity of the p- and n-metal contacts is increased [48,117,122,123]. The IV characteristics do not change with KOH etching as discussed in details elsewhere [98] (refer to Figure 6c); however, in the device discussed here the voltage increased by ~ 1 V after 50 sec KOH etching (refer to Figure 6d) which was probably due to a crack in the TFFC LED; however, further KOH etching did not affect the IV.

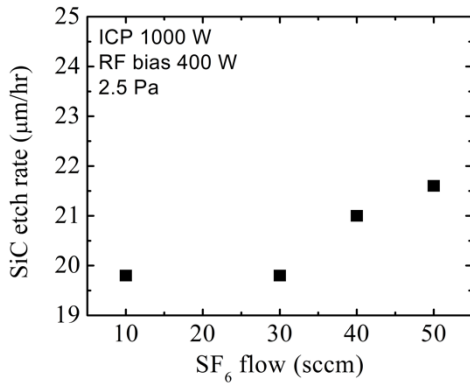
5. Conclusions

We developed a highly selective SF₆ plasma etch of SiC over AlN and a viable manufacturing method for epitaxial transfer from SiC to another substrate via wafer bonding and SiC substrate-removal by SF₆ etching. Then, we demonstrated it on UV-C LEDs that were grown on SiC to fabricate high LEE TFFC LEDs. The SiC substrate was bonded via Au-Au thermocompression bonding to another n- and p-patterned thermally conductive substrate. The growth substrate was removed by a two-step ICP etching without micromasking defects on the etched surface. The first step was a high SiC etch rate (~ 46 $\mu\text{m/hr}$) at a high RF bias power (400 W). The second step was a selective SiC etch rate (~ 7 $\mu\text{m/hr}$) at a low RF bias power (49 W), with an etch selectivity of SiC:AlN $\sim 90:1$ at a process pressure of 1.33 Pa; higher SiC:AlN etch selectivity of $\sim 150:1$ was also achieved at a lower process pressure. The highly selective SF₆ etch at low bias was essential for removing all SiC by reliably stopping at the LEDs' AlN buffer layer, which acts as an etch stop layer. We demonstrated a TFFC manufacturing method for UV-C LEDs that were grown on SiC. The LEE was significantly enhanced via KOH roughening of the exposed N-face AlN. KOH roughening enhanced the LEE by ~ 3 X for UV LEDs without encapsulation and despite the use of 5 nm p-GaN as a p-contact layer.

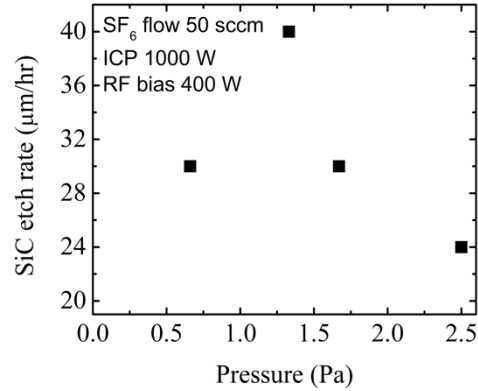
Acknowledgements

This work was funded by the King Abdulaziz City for Science and Technology (KACST), the Technology Innovations Center (TIC) program, and the KACST-KAUST-UCSB Solid State Lighting Program. The authors are appreciative of the support of the Solid State Lighting and Energy Electronics Center (SSLEEC) at UCSB. A portion of this work was conducted in the UCSB nanofabrication facility and part of the NSF NNIN network (ECS-0335765), as well as the UCSB MRL, which is supported by the NSF MRSEC Program (DMR05-20415). The authors acknowledge the UCSB-Collaborative Research in Engineering, Science and Technology (CREST) Malaysia project. This work was also supported by the National Science Foundation Graduate Research Fellowship Program (Grant No. 1650114). Any opinions, findings, and conclusions or recommendations expressed in this material are those of the author(s) and may not reflect the views of the National Science Foundation. The authors would also like to thank the cleanroom staff at UCSB nanofabrication facility, especially Brian Thibault for helpful discussions.

List of Figures

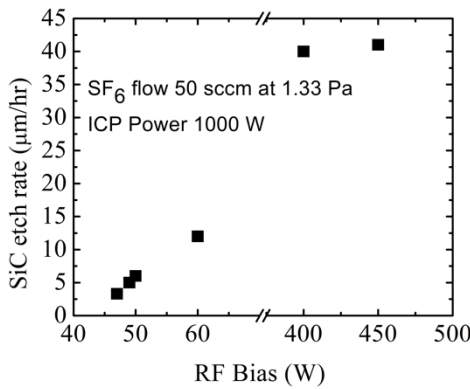


(a) Bulk SiC etch rate (μm/hr) vs SF₆ flow rate (sccm). Higher flow rate increases the etch rate and improves the lateral etch uniformity.

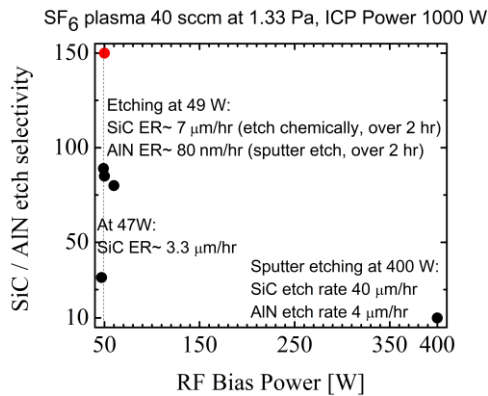


(b) Bulk SiC etch rate (μm/hr) vs pressure (Pa). The etch rate peaks at 1.33 Pa when the product of the ions' energies and the ion densities is maximum.

Figure 1. The SF₆ flow and process pressure, were examined to determine the trends between the etch parameters to optimize for a high SiC etch rate. The process parameters were fixed at 1000 W ICP, 400 RF bias, and SF₆ 50 sccm flow. The etch rates were measured for bulk SiC over a period of ~40 min – on a fused silica carrier wafer.



(a) Bulk SiC etch rate (μm/hr) vs RF bias (W).



(b) SiC:AlN etch selectivity as function of RF bias power (W).

Figure 2. In figure 2(a), at high RF bias, the SiC etch rate was dominated by sputter etching, however, at low RF bias sputter etch rate is minimal, and SiC is primarily chemically etched. Figure 2(b) shows that SiC:AlN etch selectivity has a strong dependence on RF bias below 60 W. The SiC:AlN etch selectivity at 49 W RT bias was 90:1 during a 2 hr etch, however, the selectivity decreased below 47 W. A higher SiC:AlN etch selectivity 150:1 (shown in red) was measured at a lower process pressure (0.8 Pa).

Table 1. Summary of lapping parameters used to mechanically thin SiC substrate with 9 μm diamond grid disc.

Lapping settings	Lapping etch rate
CCW 5 wafer rotation/ min 6 pad rotation /min	25-30 $\mu\text{m}/\text{min}$

Table 2. Summary of etch parameters for the two-steps ICP SF₆ etch to selectively remove SiC (using fused silica as a carrier).

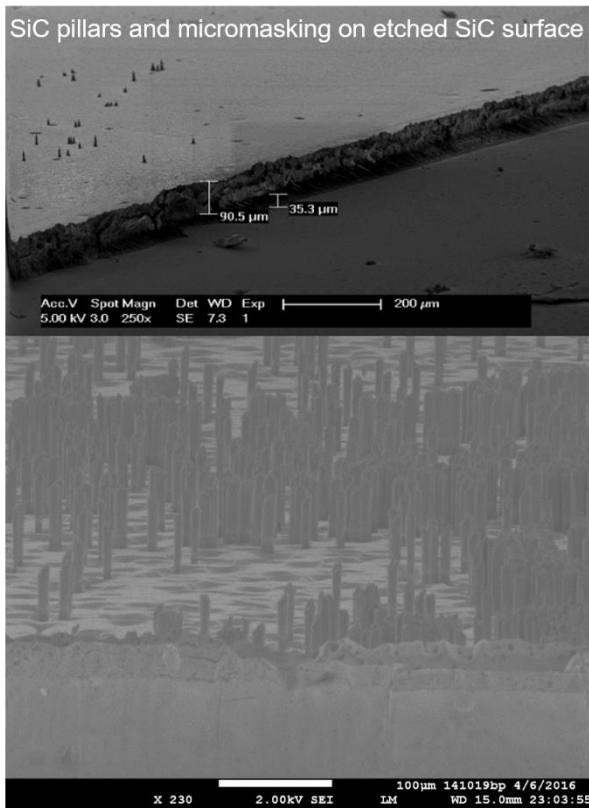
Process parameter	Fast SiC etch	Selective SiC etch (slow)
Pressure	1.33 Pa	1.33 Pa
ICP power	1000 W	1000 W
SF ₆ Flow	50 sccm	50 sccm
ICP bias	400 W	49 W
Etch rate	40 $\mu\text{m}/\text{hr}$ (40 min)	~ 7 $\mu\text{m}/\text{hr}$ (2 hr)
	46 $\mu\text{m}/\text{hr}$ (90 min)	
	47 $\mu\text{m}/\text{hr}$ (2 hr)	
SiC:AlN Selectivity	10:1	$\sim 90:1$ ($\sim 150:1$ at 0.8 Pa)
Impact on SiC surface	Rough hydrophilic SiC surface	After SiC is completely etched, the surface changes from hydrophilic to hydrophobic; smooth N-face AlN surface (RMS roughness < 1 nm) is exposed.

Table 3. Summary of the etch rate, and selectivity of SiC and various 6-inch carrier wafers used in the ICP system (at 1000 W ICP, 400 W RF bias, 1.33 Pa).

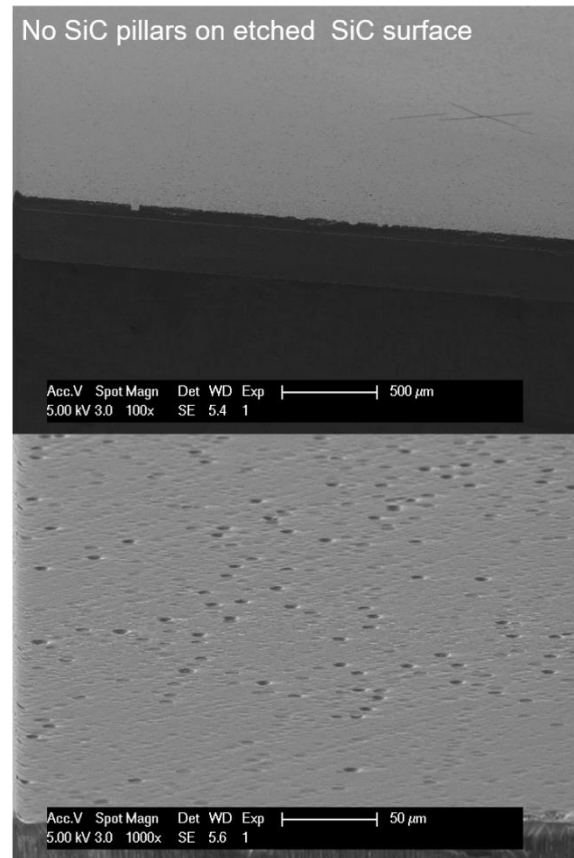
6" Carrier wafer	Etch rate ($\mu\text{m}/\text{hr}$)	SiC:Carrier wafer etch selectivity at 400 W RF bias	Cost	Comments
SiC	40	1:1	\$1000	--
Sapphire	5	8:1	\$400	Satisfactory selectivity but expensive.
Fused Silica	20	1.9:1	\$30	Satisfactory selectivity and inexpensive.
Al wafer	1.5-2	25:1	\$200	Sputter into sample and etch chamber walls
Ni wafer	1	40:1	\$200	Sputter into sample and etch chamber walls.
Cu film on Si wafer	NA	NA	NA	Sputter contaminating and nonvolatile etch byproducts into sample and etch chamber walls
Ni film on Si wafer	1	40:1	NA	Sputter into sample and etch chamber walls. Also, Ni films thicker than 2 μm buckle and delaminate due to high compressive stress.

Table 4. Summary for Au-Au thermo-compression bonding characteristics with Finetech flip-chip bonder.

Bonding type	Temperature and Force	Sample size
Au-Au thermo-compression bonding	To minimize p-mirror damage:	0.3x0.3 cm ² to 1.5x1.5 cm ²
	1-275 °C, 5 min (30 N/cm ²) 2- 200 °C, 2 hr (300 N/cm ² with graphite fixture)	



(a)



(b)

Figure 3. SiC pillars can be completely removed from the surface if appropriate process controls are applied. The image on the left (a) shows SiC pillars (40+ μm micromasking defects) that can form during etching and that will not be completely etched even when the highly selective etch is subsequently applied. The SiC pillars formation was suppressed as shown on the right (b) by an optimized etch and process controls: 1) Metal carrier wafers were avoided (fused silica carrier was employed). 2) The carrier wafer and etch chamber were seasoned with SF₆ plasma prior to etching.

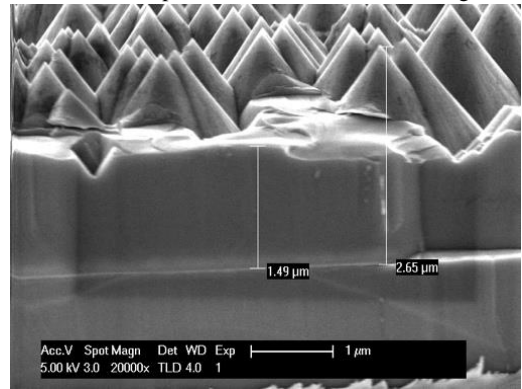
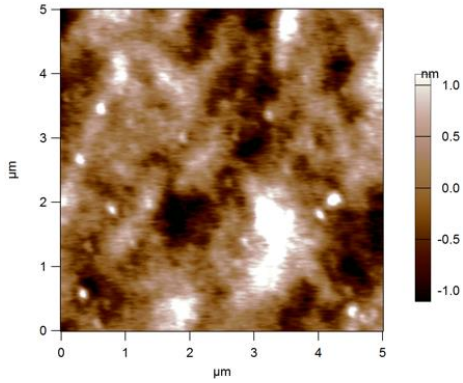
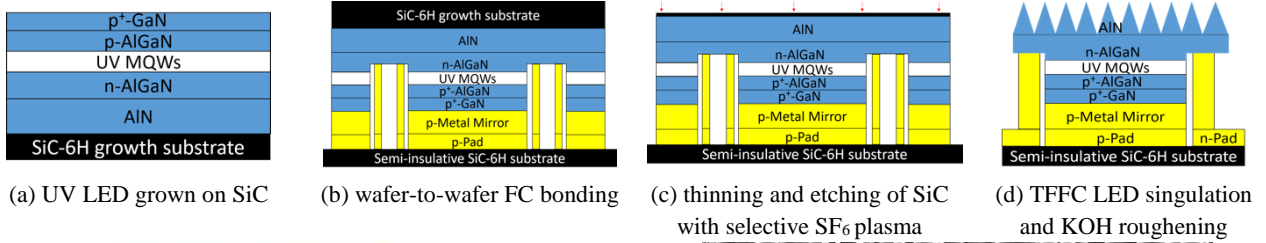
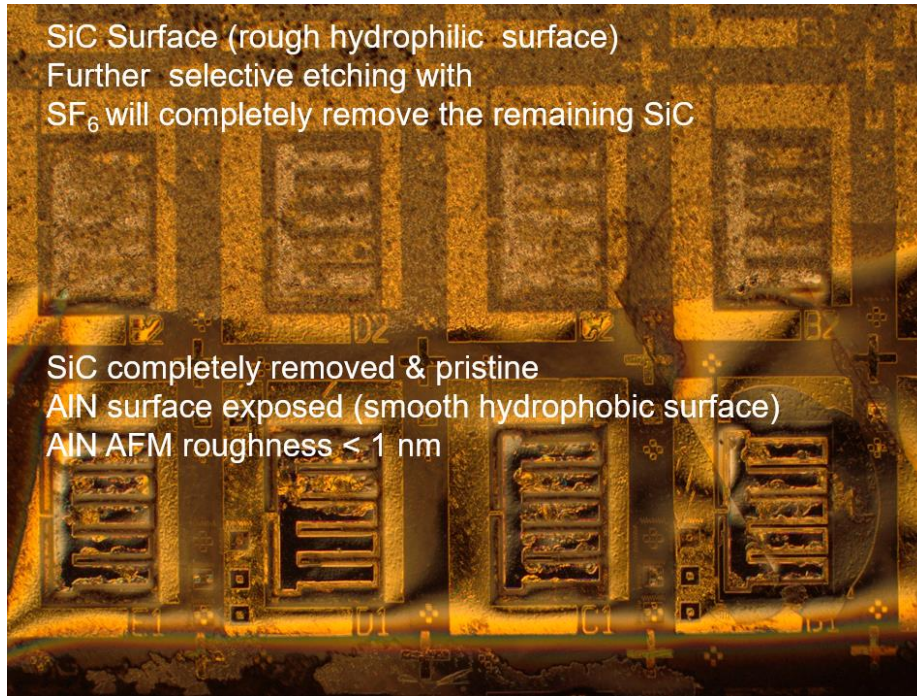
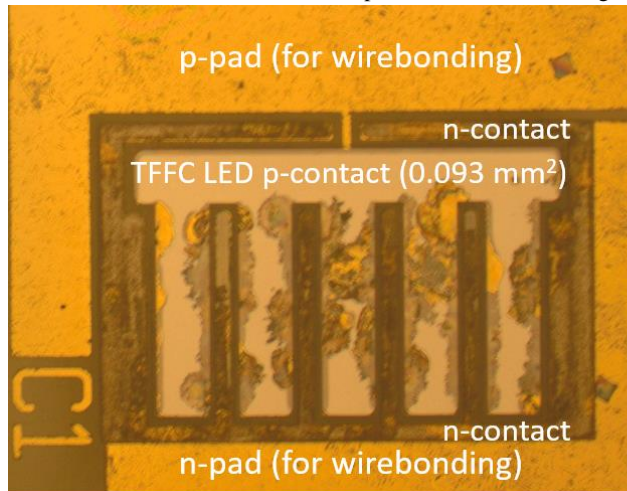


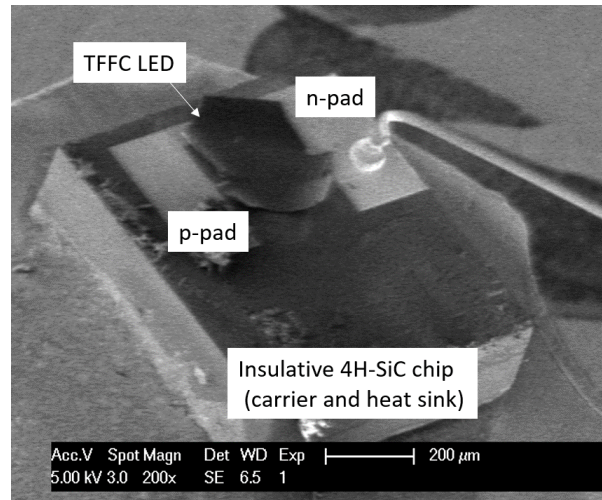
Figure 4. Process flow (a-d) demonstrate UV-C thin-film flip-chip (TFCC) grown on SiC and (e) shows AFM of exposed AIN surface after completing SiC growth substrate-removal in step (c). The hexagonal pyramids shown in (f) expand the effective angle of the light-extraction-cones. Figure adapted, with permission, from Ref. [85].



(a) Differential interference contrast (DIC) micrograph shows eight TFFC LEDs during an etch stop before the substrate is completely etched by the SF_6 plasma. In the top four LEDs, a thin layer of SiC remained. In the bottom four LEDs, no SiC remained and the N-face AlN was exposed. The colorful fringes in the lower four LEDs were due to thinfilm interference.

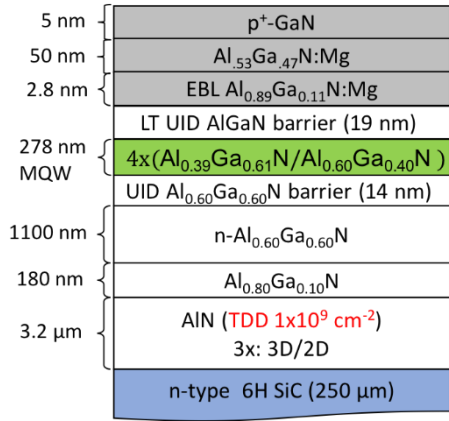


(b) Optical micrograph of UV-C TFFC LED (278 nm).

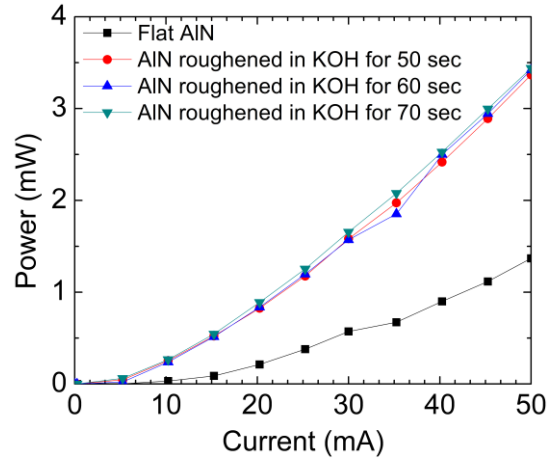


(c) SEM image of a packaged UV-C TFFC LED (278 nm).

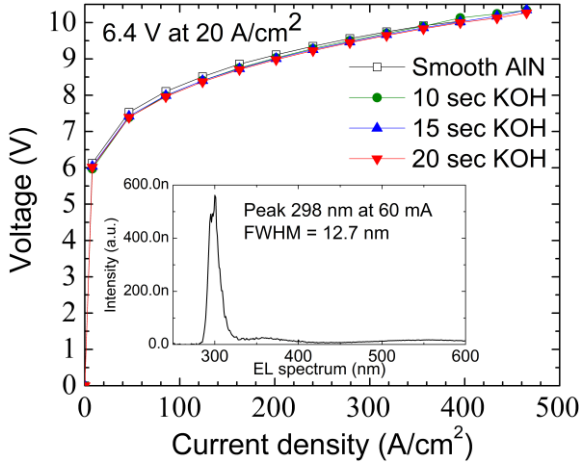
Figure 5. Optical microscope micrographs of a processed thin film LED (5-finger topology) with no cracks or chipping in the active region in (a) and (b). After dicing, the suspended AlN/AlGaIn/n-AlGaIn between the TFFC LEDs concave up due to residual tensile stresses in the AlN/AlGaIn/n-AlGaIn film which renders the n- and p- pads accessible as shown in (c).



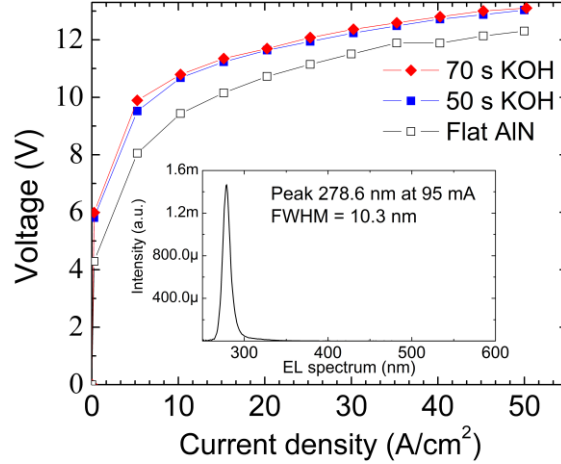
(a) 278 nm LED structure on SiC. The TDD was $\sim 1 \times 10^9$ cm^{-2} in the AlN buffer and AlGaIn layers.



(b) The light-current (L-I) curve before, and after KOH roughening. The enhancement in the L-I slope KOH roughening was $\sim 200\%$. The area of the p-contact (Ni/Al/Ni/Au) was $0.093 \text{ mm}^2 \sim 0.1 \text{ mm}^2$.



(c) The voltage-current (I-V) curve before, and after KOH roughening, for a 298 nm TFFC LED. The inset shows a 298 nm EL spectrum at 60 mA with FWHM of 12.7 nm. The area of the p-contact (Ni/Al/Ni/Au) was 0.013 mm^2 .



(d) The voltage-current (I-V) curve before, and after KOH roughening, for the 278 nm TFFC LED. The inset shows a 278.5 nm EL spectrum at 95 mA with FWHM of 10 nm. The DC power was 7.6 mW at 95 mA.

Figure 6. TFFC LEDs demonstration had high LEE. The LEE was enhanced significantly via KOH roughening of the exposed N-face AlN layer of TFFC LED. The L-I slope increased by $\sim 3X$ with optimized KOH roughening without encapsulation, and despite using 5 nm p-GaN as p-contact layer.

References

- [1] Lui G Y, Roser D, Corkish R, Ashbolt N J and Stuetz R 2016 Point-of-use water disinfection using ultraviolet and visible light-emitting diodes *Sci. Total Environ.* **553** 626–35
- [2] Song K, Mohseni M and Taghipour F 2016 Application of ultraviolet light-emitting diodes (UV-LEDs) for water disinfection: A review *Water Res.* **94** 341–9
- [3] Kheyrandish A, Mohseni M and Taghipour F 2017 Development of a method for the characterization and operation of UV-LED for water treatment *Water Res.* **122** 570–9
- [4] Vilhunen S, Särkkä H and Sillanpää M 2009 Ultraviolet light-emitting diodes in water disinfection *Environ. Sci. Pollut. Res.* **16** 439–42
- [5] Alkire B C, Raykar N P, Shrimel M G, Weiser T G, Bickler S W, Rose J A, Nutt C T, Greenberg S L M, Kotagal M, Riesel J N, Esquivel M, Uribe-Leitz T, Molina G, Roy N, Meara J G and Farmer P E 2015 Global access to surgical care: a modelling study *Lancet Glob. Heal.* **3** e316–23
- [6] Reygadas F, Gruber J S, Ray I and Nelson K L 2015 Field efficacy evaluation and post-treatment contamination risk assessment of an ultraviolet disinfection and safe storage system *Water Res.* **85** 74–84
- [7] Hutchens M P, Drennan S L and Cambronne E D 2015 Calibration of optimal use parameters for an ultraviolet light-emitting diode in eliminating bacterial contamination on needleless connectors. *J. Appl. Microbiol.* **118** 1298–305
- [8] Messina G, Fattorini M, Nante N, Rosadini D, Serafini A, Tani M and Cevenini G 2016 Time Effectiveness of Ultraviolet C Light (UVC) Emitted by Light Emitting Diodes (LEDs) in Reducing Stethoscope Contamination. *Int. J. Environ. Res. Public Health* **13**
- [9] Bolton J R and Linden K G 2003 Standardization of Methods for Fluence (UV Dose) Determination in Bench-Scale UV Experiments *J. Environ. Eng.* **129** 209–15
- [10] Destiani R, Templeton M R and Kowalski W 2018 Relative Ultraviolet Sensitivity of Selected Antibiotic Resistance Genes in Waterborne Bacteria *Environ. Eng. Sci.* **35** 770–4
- [11] Muramoto Y, Kimura M and Nouda S 2014 Development and future of ultraviolet light-emitting diodes: UV-LED will replace the UV lamp *Semicond. Sci. Technol.* **29** 084004
- [12] Hirayama H 2016 Growth Techniques of AlN/AlGa_N and Development of High-Efficiency Deep-Ultraviolet Light-Emitting Diodes pp 75–113
- [13] HIRAYAMA H, FUJIKAWA S and KAMATA N 2015 Recent Progress in AlGa_N-Based Deep-UV LEDs *Electron. Commun. Japan* **98** 1–8
- [14] Khan A, Balakrishnan K and Katona T 2008 Ultraviolet light-emitting diodes based on group three nitrides *Nat. Photonics* **2** 77–84
- [15] Wernicke T, Martens M, Kuhn C, Reich C, Mehnke F, Jeschke J, Feneber M, Rass J, Enslin J, Lapeyrade M, Zeimber U, Mogilatenko A, Einfeldt S, Kueller V, Hagedorn S, Knauer A, Hartmann C, Wollweber J, Goldhahn R, Bickermann M, Weyers M and Kneissl M 2015 Challenges for AlGa_N Based UV Laser Diodes *Light, Energy and the Environment 2015* (Washington, D.C.: OSA) p DM2D.4
- [16] Kneissl M, Kolbe T, Chua C, Kueller V, Lobo N, Stellmach J, Knauer A, Rodriguez H, Einfeldt S, Yang Z, Johnson N M and Weyers M 2011 Advances in group III-nitride-based deep UV light-emitting diode technology *Semicond. Sci. Technol.* **26** 014036
- [17] Martens M, Mehnke F, Kuhn C, Reich C, Kueller V, Knauer A, Netzel C, Hartmann C, Wollweber J, Rass J, Wernicke T, Bickermann M, Weyers M and Kneissl M 2014

- Performance characteristics of UV-C AlGaIn-based lasers grown on sapphire and bulk AlN substrates *IEEE Photonics Technol. Lett.*
- [18] Kneissl M and Rass J *III-nitride ultraviolet emitters : technology and applications*
- [19] Pegues D A, Han J, Gilmar C, McDonnell B and Gaynes S 2017 Impact of Ultraviolet Germicidal Irradiation for No-Touch Terminal Room Disinfection on Clostridium difficile Infection Incidence Among Hematology-Oncology Patients *Infect. Control Hosp. Epidemiol.* **38** 39–44
- [20] Haas J P, Menz J, Dusza S and Montecalvo M A 2014 Implementation and impact of ultraviolet environmental disinfection in an acute care setting. *Am. J. Infect. Control* **42** 586–90
- [21] S. M. Iftiqar Y L M J N B S K D and J Y 2012 *Photodiodes - From Fundamentals to Applications* ed I Yun (InTech)
- [22] Lu B and Palacios T 2010 High Breakdown (>1500 V) AlGaIn/GaN HEMTs by Substrate-Transfer Technology *IEEE Electron Device Lett.* **31** 951–3
- [23] Meyer D J, Downey B P, Katzer D S, Nepal N, Wheeler V D, Hardy M T, Anderson T J and Storm D F 2016 Epitaxial Lift-Off and Transfer of III-N Materials and Devices from SiC Substrates *IEEE Trans. Semicond. Manuf.* **29** 384–9
- [24] Shealy J B, Shealy J B, Patel P, Hodge M D, Vetry R and Shealy J R 2016 Single crystal aluminum nitride film bulk acoustic resonators 2016 *IEEE Radio and Wireless Symposium (RWS)* (IEEE) pp 16–9
- [25] Chen G, Zhao X, Wang X, Jin H, Li S, Dong S, Flewitt A J, Milne W I and Luo J K 2015 Film bulk acoustic resonators integrated on arbitrary substrates using a polymer support layer *Sci. Rep.* **5** 9510
- [26] Buchine B A, Hughes W L, Degertekin F L and Wang Z L 2006 Bulk Acoustic Resonator Based on Piezoelectric ZnO Belts *Nano Lett.* **6** 1155–9
- [27] Senesky D G and Pisano A P 2010 Aluminum nitride as a masking material for the plasma etching of silicon carbide structures 2010 *IEEE 23rd International Conference on Micro Electro Mechanical Systems (MEMS)* (IEEE) pp 352–5
- [28] Luna L E, Tadjer M J, Anderson T J, Imhoff E A, Hobart K D and Kub F J 2017 Dry Etching of High Aspect Ratio 4H-SiC Microstructures *ECS J. Solid State Sci. Technol.* **6** P207–10
- [29] Dowling K M, Ransom E H and Senesky D G 2017 Profile Evolution of High Aspect Ratio Silicon Carbide Trenches by Inductive Coupled Plasma Etching *J. Microelectromechanical Syst.* **26** 135–42
- [30] Choi J H, Latu-Romain L, Bano E, Dhalluin F, Chevolleau T and Baron T 2012 Fabrication of SiC nanopillars by inductively coupled SF₆/O₂ plasma etching *J. Phys. D. Appl. Phys.* **45** 235204
- [31] Keller S and DenBaars S P 2003 Metalorganic chemical vapor deposition of group III nitrides—a discussion of critical issues *J. Cryst. Growth* **248** 479–86
- [32] Simon J, Protasenko V, Lian C, Xing H and Jena D 2010 Polarization-induced hole doping in wide-band-gap uniaxial semiconductor heterostructures. *Science* **327** 60–4
- [33] Inoue S, Tamari N and Taniguchi M 2017 150 mW deep-ultraviolet light-emitting diodes with large-area AlN nanophotonic light-extraction structure emitting at 265 nm *Appl. Phys. Lett.* **110** 141106
- [34] Jo M, Maeda N and Hirayama H 2016 Enhanced light extraction in 260 nm light-emitting diode with a highly transparent p-AlGaIn layer *Appl. Phys. Express* **9** 012102

- [35] Shatalov M, Sun W, Lunev A, Hu X, Dobrinsky A, Bilenko Y, Yang J, Shur M, Gaska R, Moe C, Garrett G and Wraback M 2012 AlGa_N Deep-Ultraviolet Light-Emitting Diodes with External Quantum Efficiency above 10% *Appl. Phys. Express* **5** 082101
- [36] Ichikawa M, Fujioka A, Kosugi T, Endo S, Sagawa H, Tamaki H, Mukai T, Uomoto M and Shimatsu T 2016 High-output-power deep ultraviolet light-emitting diode assembly using direct bonding *Appl. Phys. Express* **9** 072101
- [37] Hirayama H 2017 Chapter Three – Growth of High-Quality AlN on Sapphire and Development of AlGa_N-Based Deep-Ultraviolet Light-Emitting Diodes *Semiconductors and Semimetals* vol 96 pp 85–120
- [38] Asif Khan M, Shatalov M, Maruska H P, Wang H M and Kuokstis E 2005 III–Nitride UV Devices *Jpn. J. Appl. Phys.* **44** 7191–206
- [39] Allerman A A, Crawford M H, Fischer A J, Bogart K H A, Lee S R, Follstaedt D M, Provencio P P and Koleske D D 2004 Growth and design of deep-UV (240–290nm) light emitting diodes using AlGa_N alloys *J. Cryst. Growth* **272** 227–41
- [40] Moustakas T D and Paiella R 2017 Optoelectronic device physics and technology of nitride semiconductors from the UV to the terahertz *Rep. Prog. Phys.* **80**
- [41] Crawford M H 2017 Chapter One – Materials Challenges of AlGa_N-Based UV Optoelectronic Devices *Semiconductors and Semimetals* vol 96 pp 3–44
- [42] Shatalov M, Jain R, Saxena T, Dobrinsky A and Shur M 2017 Development of Deep UV LEDs and Current Problems in Material and Device Technology *Semicond. Semimetals* **96** 45–83
- [43] Pernot C, Fukahori S, Inazu T, Fujita T, Kim M, Nagasawa Y, Hirano A, Ippommatsu M, Iwaya M, Kamiyama S, Akasaki I and Amano H 2011 Development of high efficiency 255-355 nm AlGa_N-based light-emitting diodes *Phys. status solidi* **208** 1594–6
- [44] Li D, Jiang K, Sun X and Guo C 2018 AlGa_N photonics: recent advances in materials and ultraviolet devices *Adv. Opt. Photonics* **10** 43
- [45] Takano T, Mino T, Sakai J, Noguchi N, Tsubaki K and Hirayama H 2017 Deep-ultraviolet light-emitting diodes with external quantum efficiency higher than 20% at 275 nm achieved by improving light-extraction efficiency *Appl. Phys. Express* **10** 031002
- [46] Guo Y, Zhang Y, Yan J, Xie H, Liu L, Chen X, Hou M, Qin Z, Wang J and Li J 2017 Light extraction enhancement of AlGa_N-based ultraviolet light-emitting diodes by substrate sidewall roughening *Appl. Phys. Lett.* **111** 011102
- [47] Yun J and Hirayama H 2017 Investigation of the light-extraction efficiency in 280 nm AlGa_N-based light-emitting diodes having a highly transparent p-AlGa_N layer *J. Appl. Phys.* **121** 013105
- [48] Ryu H-Y, Choi I-G, Choi H-S and Shim J-I 2013 Investigation of Light Extraction Efficiency in AlGa_N Deep-Ultraviolet Light-Emitting Diodes *Appl. Phys. Express* **6** 062101
- [49] Rass J and Lobo-Ploch N 2016 Optical Polarization and Light Extraction from UV LEDs (Springer, Cham) pp 137–70
- [50] Grandusky J R, Chen J, Gibb S R, Mendrick M C, Moe C G, Rodak L, Garrett G A, Wraback M and Schowalter L J 2013 270 nm Pseudomorphic Ultraviolet Light-Emitting Diodes with Over 60 mW Continuous Wave Output Power *Appl. Phys. Express* **6** 032101
- [51] Inazu T, Fukahori S, Pernot C, Kim M H, Fujita T, Nagasawa Y, Hirano A, Ippommatsu M, Iwaya M, Takeuchi T, Kamiyama S, Yamaguchi M, Honda Y, Amano H and Akasaki I 2011 Improvement of Light Extraction Efficiency for AlGa_N-Based Deep Ultraviolet

- Light-Emitting Diodes *Jpn. J. Appl. Phys.* **50** 122101
- [52] Tran B T and Hirayama H 2017 Growth and Fabrication of High External Quantum Efficiency AlGa_N-Based Deep Ultraviolet Light-Emitting Diode Grown on Pattern Si Substrate *Sci. Rep.* **7** 12176
- [53] Zhang Y, Allerman A A, Krishnamoorthy S, Akyol F, Moseley M W, Armstrong A M and Rajan S 2016 Enhanced light extraction in tunnel junction-enabled top emitting UV LEDs *Appl. Phys. Express* **9** 052102
- [54] Zhang Y, Krishnamoorthy S, Akyol F, Bajaj S, Allerman A A, Moseley M W, Armstrong A M and Rajan S 2017 Tunnel-injected sub-260 nm ultraviolet light emitting diodes *Appl. Phys. Lett.* **110** 201102
- [55] Muth J F, Lee J H, Shmagin I K, Kolbas R M, Jr. H C C, Keller B P, Mishra U K and DenBaars S P 1997 Absorption coefficient, energy gap, exciton binding energy, and recombination lifetime of GaN obtained from transmission measurements *Appl. Phys. Lett.* **71** 2572
- [56] Nam K B, Li J, Nakarmi M L M, Lin J Y and Jiang H X 2004 Unique optical properties of AlGa_N alloys and related ultraviolet emitters *Appl. Phys. Lett.* **84** 5264
- [57] Nakashima T, Takeda K, Iwaya M, Takeuchi T, Kamiyama S, Akasaki I and Amano H 2014 Improvement of light extraction efficiency of 350-nm emission UV light-emitting diodes *Phys. status solidi* **11** 836–9
- [58] Rass J and Lobo-Ploch N 2016 Optical Polarization and Light Extraction from UV LEDs pp 137–70
- [59] Schubert E F 2015 *Physical Foundations of Solid-State Devices* (E. Fred Schubert)
- [60] Kitai A 2011 *Principles of Solar Cells, LEDs and Diodes: The role of the PN junction* (Chichester, UK: John Wiley & Sons, Ltd)
- [61] Yamada K, Furusawa Y, Nagai S, Hirano A, Ippommatsu M, Aosaki K, Morishima N, Amano H and Akasaki I 2015 Development of underfilling and encapsulation for deep-ultraviolet LEDs *Appl. Phys. Express* **8** 012101
- [62] Nagai S, Yamada K, Hirano A, Ippommatsu M, Ito M, Morishima N, Aosaki K, Honda Y, Amano H and Akasaki I 2016 Development of highly durable deep-ultraviolet AlGa_N-based LED multichip array with hemispherical encapsulated structures using a selected resin through a detailed feasibility study *Jpn. J. Appl. Phys.* **55** 082101
- [63] Peng Y, Guo X, Liang R, Cheng H and Chen M 2017 Enhanced Light Extraction from DUV-LEDs by AlN-Doped Fluoropolymer Encapsulation *IEEE Photonics Technol. Lett.* 1–1
- [64] Grandusky J R, Chen J, Gibb S R, Mendrick M C, Moe C G, Rodak L, Garrett G A, Wraback M and Schowalter L J 2013 270 nm Pseudomorphic Ultraviolet {Light-Emitting} Diodes with Over 60 {mW} Continuous Wave Output Power *Appl. Phys. Express* **6**
- [65] Kinoshita T, Hironaka K, Obata T, Nagashima T, Dalmau R, Schlessner R, Moody B, Xie J, Inoue S, Kumagai Y, Koukitu A and Sitar Z 2012 Deep-Ultraviolet Light-Emitting Diodes Fabricated on AlN Substrates Prepared by Hydride Vapor Phase Epitaxy *Appl. Phys. Express* **5** 122101
- [66] Adivarahan V, Chitnis A, Zhang J P, Shatalov M, Yang J W, Simin G, Khan M A, Gaska R and Shur M S 2001 Ultraviolet light-emitting diodes at 340 nm using quaternary AlInGa_N multiple quantum wells *Appl. Phys. Lett.* **79** 4240–2
- [67] Moe C G 2007 Growth and fabrication of deep ultraviolet light emitting diodes on silicon

- carbide substrates *ProQuest Diss. Theses; Ph.D.*
- [68] Vampola K 2009 Improvement of III-N visible and ultraviolet light-emitting diode performance, including extraction efficiency, electrical efficiency, thermal management and efficiency maintenance at high current densities. *ProQuest Diss. Theses; Ph.D.*
- [69] Park J-S, Fothergill D W, Wellenius P, Bishop S M, Muth J F and Davis R F 2006 Origins of Parasitic Emissions from 353 nm AlGaIn-based Ultraviolet Light Emitting Diodes over SiC Substrates *Jpn. J. Appl. Phys.* **45** 4083–6
- [70] Chakraborty A, Moe C G, Wu Y, Mates T, Keller S, Speck J S, DenBaars S P and Mishra U K 2007 Electrical and structural characterization of Mg-doped p-type Al_{0.69}Ga_{0.31}N films on SiC substrate *J. Appl. Phys.* **101** 053717
- [71] Zhang W, Nikiforov A Y, Thomidis C, Woodward J, Sun H, Kao C-K, Bhattarai D, Moldawer A, Zhou L, Smith D J and Moustakas T D 2012 Molecular beam epitaxy growth of AlGaIn quantum wells on 6H-SiC substrates with high internal quantum efficiency *J. Vac. Sci. Technol. B, Nanotechnol. Microelectron. Mater. Process. Meas. Phenom.* **30** 02B119
- [72] Liang H, Tao P, Xia X, Chen Y, Zhang K, Liu Y, Shen R, Luo Y, Zhang Y and Du G 2016 Vertically conducting deep-ultraviolet light-emitting diodes with interband tunneling junction grown on 6H-SiC substrate *Jpn. J. Appl. Phys.* **55** 031202
- [73] Taniyasu Y, Kasu M and Makimoto T 2006 An aluminium nitride light-emitting diode with a wavelength of 210 nanometres *Nature* **441** 325–8
- [74] Kawanishi H, Senuma M and Nukui T 2006 Anisotropic polarization characteristics of lasing and spontaneous surface and edge emissions from deep-ultraviolet ($\lambda \approx 240\text{nm}$) AlGaIn multiple-quantum-well lasers *Appl. Phys. Lett.* **89** 041126
- [75] Okumura H, Kimoto T and Suda J 2014 Formation mechanism of threading-dislocation array in AlN layers grown on 6H-SiC (0001) substrates with 3-bilayer-high surface steps *Appl. Phys. Lett.* **105** 071603
- [76] Okumura H, Kimoto T and Suda J 2012 Over-700-nm Critical Thickness of AlN Grown on 6H-SiC(0001) by Molecular Beam Epitaxy *Appl. Phys. Express* **5** 105502
- [77] Okumura H, Kimoto T and Suda J 2011 Reduction of Threading Dislocation Density in 2H-AlN Grown on 6H-SiC(0001) by Minimizing Unintentional Active-Nitrogen Exposure before Growth *Appl. Phys. Express* **4** 025502
- [78] Chen Z, Newman S, Brown D, Chung R, Keller S, Mishra U K, Denbaars S P and Nakamura S 2008 High quality AlN grown on SiC by metal organic chemical vapor deposition *Appl. Phys. Lett.* **93** 191906
- [79] Liu L and Edgar J H 2002 Substrates for gallium nitride epitaxy *Mater. Sci. Eng. R Reports* **37** 61–127
- [80] Edmond J, Abare A, Bergman M, Bharathan J, Lee Bunker K, Emerson D, Haberern K, Ibbetson J, Leung M, Russel P and Slater D 2004 High efficiency GaN-based LEDs and lasers on SiC *J. Cryst. Growth* **272** 242–50
- [81] Foronda H M, Wu F, Zollner C, Alif M E M E, SaifAddin B, Almogbel A, Iza M, Nakamura S, DenBaars S P and Speck J S 2018 Low threading dislocation density aluminum nitride on silicon carbide through the use of reduced temperature interlayers *J. Cryst. Growth* **483** 134–9
- [82] SaifAddin B, Foronda H, Yonkee B, Cantore M, Oh S H, Farrell R, Margalith T, Young E C, Nakamura S, DenBaars S P and Speck J S 2015 Nanostructure Patterning of AlN Surface and Removal of SiC Substrates for High Extraction Efficiency Thin Film UV

- LEDs (Late News) *42nd Int. Symp. Compd. Semicond. St. Barbar. CA.*
- [83] SaifAddin B K, Foronda H, Michael Iza, Nakamura S, DenBaars S P and Speck J S 2016 Epi-Transfer Technology for High EQE UV LEDs Grown on SiC (Late News) *MRS Int. Work. Nitride Semicond. (IWN 2016). Orlando, FL.*
- [84] SaifAddin B K, Foronda H, Almogbel A, Zollner C J, Iza M, Nakamura S, Denbaars S P and Speck J S 2017 First demonstration of lateral thin-film flip-chip ultraviolet light emitting diodes grown on SiC (Late News) *12th International Conference on Nitride Semiconductors (ICNS 12) (Strasbourg, France)*
- [85] SaifAddin B K, Zollner C J, Almogbel A, Foronda H, Wu F, Albadri A, Al Yamani A, Iza M, Nakamura S, Denbaars S P and Speck J S 2018 Developments in AlGa_N and UV-C LEDs grown on SiC *Proceedings of SPIE - The International Society for Optical Engineering* vol 10554
- [86] Fujii T, Gao Y, Sharma R, Hu E L, DenBaars S P and Nakamura S 2004 Increase in the extraction efficiency of GaN-based light-emitting diodes via surface roughening *Appl. Phys. Lett.* **84** 855
- [87] Shchekin O B, Epler J E, Trottier T A, Margalith T, Steigerwald D A, Holcomb M O, Martin P S and Krames M R 2006 High performance thin-film flip-chip InGa_N-Ga_N light-emitting diodes **89** 071109
- [88] Krames M R, Shchekin O B, Mueller-Mach R, Mueller G O, Zhou L, Harbers G and Craford M G 2007 Status and future of high-power light-emitting diodes for solid-state lighting *IEEE/OSA J. Disp. Technol.*
- [89] Zhou L, Epler J E, Krames M R, Goetz W, Gherasimova M, Ren Z, Han J, Kneissl M and Johnson N M 2006 Vertical injection thin-film AlGa_N/AlGa_N multiple-quantum-well deep ultraviolet light-emitting diodes *Appl. Phys. Lett.* **89** 241113
- [90] Adivarahan V, Heidari A, Zhang B, Fareed Q, Hwang S, Islam M and Khan A 2009 280 nm Deep Ultraviolet Light Emitting Diode Lamp with an AlGa_N Multiple Quantum Well Active Region *Appl. Phys. Express* **2** 102101
- [91] Hwang S, Morgan D, Kesler A, Lachab M, Zhang B, Heidari A, Nazir H, Ahmad I, Dion J, Fareed Q, Adivarahan V, Islam M and Khan A 2011 276 nm Substrate-Free Flip-Chip AlGa_N Light-Emitting Diodes *Appl. Phys. Express* **4** 032102
- [92] Aoshima H, Takeda K, Takehara K, Ito S, Mori M, Iwaya M, Takeuchi T, Kamiyama S, Akasaki I and Amano H 2012 Laser lift-off of AlN/sapphire for UV light-emitting diodes *Phys. status solidi* **9** 753–6
- [93] Lachab M, Asif F, Zhang B, Ahmad I, Heidari A, Fareed Q, Adivarahan V and Khan A 2013 Enhancement of light extraction efficiency in sub-300nm nitride thin-film flip-chip light-emitting diodes *Solid. State. Electron.* **89** 156–60
- [94] Cho H K, Krüger O, Külberg A, Rass J, Zeimer U, Kolbe T, Knauer A, Einfeldt S, Weyers M and Kneissl M 2017 Chip design for thin-film deep ultraviolet LEDs fabricated by laser lift-off of the sapphire substrate *Semicond. Sci. Technol.* **32** 12LT01
- [95] Wong W S, Sands T, Cheung N W, Kneissl M, Bour D P, Mei P, Romano L T and Johnson N M 1999 Fabrication of thin-film InGa_N light-emitting diode membranes by laser lift-off *Appl. Phys. Lett.* **75** 1360
- [96] Yonkee B P, SaifAddin B K, Leonard J T, DenBaars S P and Nakamura S 2016 Flip-chip blue LEDs grown on bulk Ga_N substrates utilizing photoelectrochemical etching for substrate removal *Appl. Phys. Express* **9** 56502
- [97] Hwang D, Yonkee B P, Burhan SaifAddin, Farrell R M, Nakamura S, Speck J S and

- DenBaars S 2016 Photoelectrochemical liftoff of LEDs grown on freestanding c-plane GaN substrates *Opt. Express* **24** 22875–80
- [98] SaifAddin Burhan, Iza Michael, Foronda Humberto, Almogbel Abdullah, Zollner Chris, Albadri Abdulrahman, AlYamani Ahmed, Nakamura Shuji, DenBaars Steven P. S J S 2018 First demonstration of high light-extraction thin-film flip-chip ultraviolet light emitting diodes grown on silicon carbide *Opt. Express*
- [99] Tsau C H, Spearing S M and Schmidt M A 2004 Characterization of Wafer-Level Thermocompression Bonds *J. Microelectromechanical Syst.* **13** 963–71
- [100] Goorsky M S, Schjølberg-Henriksen K, Beekley B, Bai T, Mani K, Ambhore P, Bajwa A, Malik N and Iyer S S 2018 Characterization of interfacial morphology of low temperature, low pressure Au–Au thermocompression bonding *Jpn. J. Appl. Phys.* **57** 02BC03
- [101] Leerungnawarat P, Hays D C, Cho H, Pearton S J, Strong R M, Zetterling C-M and Östling M 1999 Via-hole etching for SiC *J. Vac. Sci. Technol. B Microelectron. Nanom. Struct. Process. Meas. Phenom.* **17** 2050
- [102] Khan F A and Adesida I 1999 High rate etching of SiC using inductively coupled plasma reactive ion etching in SF₆-based gas mixtures *Appl. Phys. Lett.* **75** 2268
- [103] Cho H, Leerungnawarat P, Hays D C, Pearton S J, Chu S N G, Strong R M, Zetterling C-M, Östling M and Ren F 2000 Ultradeep, low-damage dry etching of SiC *Appl. Phys. Lett.* **76** 739
- [104] Chabert P, Cunge G, Booth J-P and Perrin J 2001 Reactive ion etching of silicon carbide in SF₆ gas: Detection of CF, CF₂, and SiF₂ etch products *Appl. Phys. Lett.* **79** 916–8
- [105] Salimian S and III C B C 1988 Selective dry etching of GaAs over AlGaAs in SF₆/SiCl₄ mixtures *J. Vac. Sci. Technol. B Microelectron. Nanom. Struct.* **6** 1641
- [106] Seaward K L, Moll N J, Coulman D J and Stickle W F 1987 An analytical study of etch and etch-stop reactions for GaAs on AlGaAs in CCl₂F₂ plasma *J. Appl. Phys.* **61** 2358–64
- [107] Epple J H, Sanchez C, Chung T, Cheng K Y and Hsieh K C 2002 Dry etching of GaP with emphasis on selective etching over AlGaP *J. Vac. Sci. Technol. B Microelectron. Nanom. Struct.* **20** 2252
- [108] Hönl S, Hahn H, Baumgartner Y, Czornomaz L and Seidler P 2018 Highly selective dry etching of GaP in the presence of Al_xGa_{1-x}P with a SiCl₄/SF₆ plasma *J. Phys. D. Appl. Phys.* **51** 185203
- [109] Nishino S, Ibaraki A, Matsunami H and Tanaka T 1980 Blue-Emitting Diodes of 6H-SiC Prepared by Chemical Vapor Deposition *Jpn. J. Appl. Phys.* **19** L353–6
- [110] Feynman R P, Leighton R B and Sands M L 1986 *The Feynman lectures on physics* (Narosa Pub. House)
- [111] Hao G-D, Taniguchi M, Tamari N and Inoue S 2016 Enhanced wall-plug efficiency in AlGaIn-based deep-ultraviolet light-emitting diodes with uniform current spreading *p*-electrode structures *J. Phys. D. Appl. Phys.* **49** 235101
- [112] SaifAddin B K 2018 Development of Deep Ultraviolet (UV-C) Thin-Film Light-Emitting Diodes Grown on SiC *ProQuest Diss. Theses; Ph.D.*
- [113] Lee K H, Park H J, Kim S H, Asadirad M, Moon Y-T, Kwak J S and Ryou J-H 2015 Light-extraction efficiency control in AlGaIn-based deep-ultraviolet flip-chip light-emitting diodes: a comparison to InGaIn-based visible flip-chip light-emitting diodes *Opt. Express* **23** 20340
- [114] Northrup J E, Chua C L, Yang Z, Wunderer T, Kneissl M, Johnson N M and Kolbe T

- 2012 Effect of strain and barrier composition on the polarization of light emission from AlGa_N/AlN quantum wells *Appl. Phys. Lett.* **100** 021101
- [115] Reich C, Guttman M, Feneberg M, Wernicke T, Mehnke F, Kuhn C, Rass J, Lapeyrade M, Einfeldt S, Knauer A, Kueller V, Weyers M, Goldhahn R and Kneissl M 2015 Strongly transverse-electric-polarized emission from deep ultraviolet AlGa_N quantum well light emitting diodes *Appl. Phys. Lett.*
- [116] Lachab M, Sun W, Jain R, Dobrinsky A, Gaevski M, Rumyantsev S, Shur M and Shatalov M 2017 Optical polarization control of photo-pumped stimulated emissions at 238 nm from AlGa_N multiple-quantum-well laser structures on AlN substrates *Appl. Phys. Express* **10** 012702
- [117] Lalau Keraly C, Kuritzky L, Cochet M and Weisbuch C 2013 Light Extraction Efficiency Part A. Ray Tracing for Light Extraction Efficiency (LEE) Modeling in Nitride LEDs (Springer, Dordrecht) pp 231–69
- [118] David A 2013 Surface-Roughened Light-Emitting Diodes: An Accurate Model *J. Disp. Technol.* **9** 301–16
- [119] Zhang Y, Krishnamoorthy S, Akyol F, Allerman A A, Moseley M W, Armstrong A M and Rajan S 2016 Design and demonstration of ultra-wide bandgap AlGa_N tunnel junctions *Appl. Phys. Lett.* **109** 121102
- [120] Rajan S and Takeuchi T 2017 III-Nitride Tunnel Junctions and Their Applications (Springer, Singapore) pp 209–38
- [121] Yonkee B P, Young E C, DenBaars S P, Nakamura S and Speck J S 2016 Silver free III-nitride flip chip light-emitting-diode with wall plug efficiency over 70% utilizing a GaN tunnel junction *Appl. Phys. Lett.* **109** 191104
- [122] Lee K H, Moon Y-T, Song J-O and Kwak J S 2015 Light interaction in sapphire/MgF₂/Al triple-layer omnidirectional reflectors in AlGa_N-based near ultraviolet light-emitting diodes. *Sci. Rep.* **5** 9717
- [123] David A 2013 Surface-Roughened Light-Emitting Diodes: An Accurate Model *J. Disp. Technol.* **9** 301–16